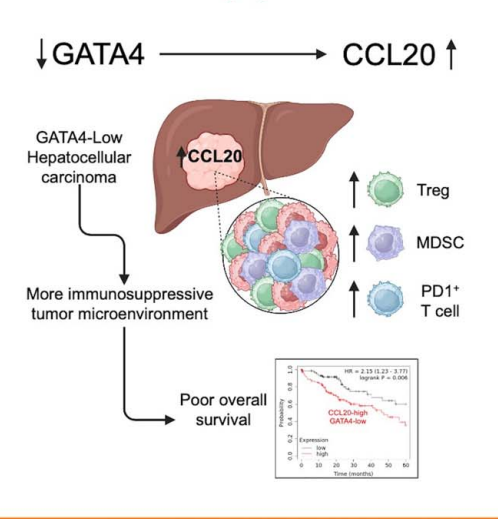


GATA4 downregulation enhances CCL20-mediated immunosuppression in hepatocellular carcinoma

VISUAL ABSTRACT

GATA4 Downregulation Enhances CCL20-Mediated Immunosuppression in Hepatocellular Carcinoma



- GATA4-low HCC tumors show increased PD-1⁺ T cells, Tregs, and MDSCs.
- GATA4 downregulation enhances the level of CCL20, a known immunosuppressive chemokine.
- CCL20 induces tumor infiltration of Tregs and MDSCs, driving immunosuppression.
- Reduced GATA4 and high CCL20 associate with poorer HCC prognosis.



DOI: 10.1097/HC9.0000000000000508

ORIGINAL ARTICLE





GATA4 downregulation enhances CCL20-mediated immunosuppression in hepatocellular carcinoma

N. Jannah M. Nasir ^{1,2}
Rebecca Ba ³ Mei Chee Lim ^{2,3} Joelle Chua ³ Phuong H. D. Nguyen ¹
Chun J. Lim ¹ Martin Wasser ¹ Sharifah N. Hazirah ¹ Tony K. H. Lim ^{2,4}
Wei Qiang Leow ^{2,4} Tracy Jiezhen Loh ^{2,4} Wei Keat Wan ^{2,4} Yin Huei Pang ⁵
Gwyneth Soon ⁵ Peng Chung Cheow ^{2,6} Juinn Huar Kam ^{2,6} Shridhar Iyer ⁷
Alfred Kow ⁷ Yock Young Dan ^{8,9} Glenn K. Bonney ⁷ Alexander Chung ^{2,6}
Brian K. P. Goh ^{2,6} Pierce K. H. Chow ^{2,6,10} Salvatore Albani ¹
Weiwei Zhai ^{11,12,13} John F. Ouyang ² Han Chong Toh ^{2,3} Valerie Chew ^{1,2} o

¹Translational Immunology Institute (TII), SingHealth-DukeNUS Academic Medical Centre, Singapore

Abbreviations: BHMT, betaine-homocysteine S-methyltransferase; CCL11, C-C Motif Chemokine Ligand 11; CCL2, C-C Motif Chemokine Ligand 2; CCL20, C-C Motif Chemokine Ligand 20; CCL21, C-C Motif Chemokine Ligand 21; CCR6, C-C Motif Chemokine Receptor 6; CIRB, Central Institution Review Board; CNTN1, contactin 1; COMP, cartilage oligomeric matrix protein; CRYAA, crystallin alpha A; CTLA4, cytotoxic T lymphocyte-associated protein 4; CXCL10, C-X-C Motif Chemokine Ligand 10; CXCL9, C-X-C Motif Chemokine Ligand 9; CyTOF, cytometry by time-of-flight; DEG, differentially enriched genes; EGA, European Genome-phenome Archive; FBXW10, F-box and WD repeat domain containing 10; FC, fold change; FFPE, formalin-fixed paraffin-embedded; FNDC5, fibronectin type III domain containing 5; FoxP3, FoxP3, Foxhead box P3; FXYD3, FXYD domain containing ion transport regulator 3; GATA4, GATA binding protein 4; GzmB, granzyme B; HAO2, hydroxyacid oxidase 2; HAVCR2, hepatitis A virus cellular receptor 2; HSPA6, heat shock protein family A (Hsp70) member 6; IGFALS, insulin-like growth factor binding protein acid labile subunit; MDSCs, myeloid-derived suppressor cell; mIF, multiplexed immunofluorescence; MMP12, matrix metallopeptidase 12; MUC13, mucin 13; NCCS, National Cancer Centre Singapore; NK, natural killer cells; NUH, National University Hospital; OS, overall survival; PD-1, programmed cell death protein 1; PDCD1, Programmed Cell Death 1; RNA-seq, RNA sequencing; SGH, Singapore General Hospital; SPP1, secreted phosphoprotein 1; Tbet, T-box transcription factor TBX21; TCGA, the Cancer Genome Atlas; TCP10L, t-complex 10 like; TIE2, tunica intima endothelial kinase 2; TIGIT, T-cell immunoreceptor with Ig and ITIM domains; TIM-3, T-cell immunoglobulin domain and mucin domain 3; TMA, tissue microarray; TME, tumor microenvironment; Tregs, regulatory T cells.

N. Jannah M. Nasir, Samuel Chuah, and Timothy Shuen share first authorship.

Supplemental Digital Content is available for this article. Direct URL citations are provided in the HTML and PDF versions of this article on the journal's website, www.hepcommjournal.com.

This is an open access article distributed under the terms of the Creative Commons Attribution-Non Commercial-No Derivatives License 4.0 (CCBY-NC-ND), where it is permissible to download and share the work provided it is properly cited. The work cannot be changed in any way or used commercially without permission from the journal.

Copyright © 2024 The Author(s). Published by Wolters Kluwer Health, Inc. on behalf of the American Association for the Study of Liver Diseases.

²Duke-NUS Medical School, Singapore

³Division of Medical Oncology, National Cancer Centre Singapore, Singapore

⁴Department of Anatomical Pathology, Singapore General Hospital, Singapore

⁵Department of Pathology, National University Hospital, Singapore

⁶Department of Hepatopancreatobiliary and Transplant Surgery, Division of Surgery and Surgical Oncology, Singapore General Hospital and National Cancer Centre Singapore, Singapore

⁷Department of Surgery, Division of Hepatobiliary and Pancreatic Surgery, University Surgical Cluster, National University Health System, Singapore

⁸Department of Medicine, Division of Gastroenterology & Hepatology, National University Hospital, Singapore

⁹Department of Medicine, Yong Loo Lin School of Medicine, National University of Singapore, Singapore

¹⁰Program in Clinical and Translational Liver Cancer Research, Division of Medical Science, National Cancer Centre, Singapore

¹¹Genome Institute of Singapore (GIS), Agency for Science, Technology and Research (A*STAR), Singapore

¹²Key Laboratory of Zoological Systematics and Evolution, Institute of Zoology, Chinese Academy of Sciences, Beijing, China

¹³Center for Excellence in Animal Evolution and Genetics, Chinese Academy of Sciences, Kunming, Yunan, China

Correspondence

Valerie Chew, Translational Immunology Institute (TII), SingHealth-DukeNUS Academic Medical Centre, Singapore 169856, Singapore.

Email: valerie.chew@duke-nus.edu.sg

Han Chong Toh, Division of Medical Oncology, National Cancer Centre Singapore 169610, Singapore.

Email: toh.han.chong@singhealth.com.sg

Abstract

Background: Hepatocellular carcinoma (HCC) is a deadly cancer with a high global mortality rate, and the downregulation of GATA binding protein 4 (*GATA4*) has been implicated in HCC progression. In this study, we investigated the role of GATA4 in shaping the immune landscape of HCC.

Methods: HCC tumor samples were classified into "low" or "normal/high" based on *GATA4* RNA expression relative to adjacent non-tumor liver tissues. The immune landscapes of *GATA4*-low and *GATA4*-normal/high tumors were analyzed using cytometry by time-of-flight, bulk/spatial transcriptomic analyses and validated by multiplex immuno-fluorescence.

Results: *GATA4*-low tumors displayed enrichment in exhausted programmed cell death protein 1+ T cells, immunosuppressive regulatory T cells, myeloid-derived suppressor cells, and macrophages, highlighting the impact of GATA4 downregulation on immunosuppression. Spatial and bulk transcriptomic analyses revealed a negative correlation between *GATA4* and C-C Motif Chemokine Ligand 20 (*CCL20*) expression in HCC. Overexpressing GATA4 confirmed CCL20 as a downstream target, contributing to an immunosuppressive tumor microenvironment, as evidenced by increased regulatory T cells and myeloid-derived suppressor cells in CCL20-high tumors. Lastly, the reduced expression of *GATA4* and higher expression of *CCL20* were associated with poorer overall survival in patients with HCC, implicating their roles in tumor progression.

Conclusions: Our study reveals that GATA4 downregulation contributes to an immunosuppressive microenvironment, driven by CCL20-mediated enrichment of regulatory T cells and myeloid-derived suppressor cells in HCC. These findings underscore the critical role of GATA4 reduction in promoting immunosuppression and HCC progression.

INTRODUCTION

Primary liver cancer is the sixth most prevalent cancer globally, with more than 900,000 cases and approximately 830,000 deaths reported in 2020, reflecting its high mortality rate. HCC accounts for 75%–85% of liver cancer cases, while the rest of the cases are composed of intrahepatic cholangiocarcinoma (10%–15%) and other rare types. Several etiologies, such as HBV and HCV infection, excessive alcohol consumption, and type 2 diabetes, are associated with the development of HCC. In recent years, immune checkpoint inhibitor combinations have become the standard of care for advanced HCC. However, immunotherapy is highly dependent on the function of immune cells, which are often suppressed in the HCC tumor microenvironment (TME).

GATA binding protein 4 (GATA4) is a transcription factor that is commonly expressed in mesodermal and endodermal tissues such as the liver and acts as a regulator of tissue development differentiation.[3] GATA4 has been shown to promote the senescence-associated secretory phenotype, a key inflammatory response important for aging and tumor promotion.[4,5] The frequent loss of GATA4, also a known tumor suppressor gene, has been reported in various cancers, including HCC.[3] More than 60% of HCC cases show a chromosomal structural loss in the short arm of chromosome 8, where GATA4 was identified as the key targeted gene. [6] The loss of GATA4 has been implicated in cancer progression and malignancy. Conditional deletion of GATA4 allele in a transgenic murine model produced mice with significantly enlarged livers exhibiting fatty liver phenotypes

and a hepatocyte gene expression profile similar to that observed in HCC.^[6] In addition, a recent study found that GATA4-mediated senescence-associated secretory phenotype may suppress tumor growth via enhanced recruitment of cytotoxic CD8 T cells,^[7] suggesting that the loss of *GATA4* leads to a poorer antitumor immune response.

In this study, we aimed to elucidate the immune landscape of HCC with respect to the expression of *GATA4* in the tumors and to determine how *GATA4* shapes the HCC TME.^[8,9] Investigating the impact of *GATA4* on the immune landscape of HCC is important and may provide new insights into the mechanisms of immunosuppression in HCC with implications for future immunotherapeutic strategies.

METHODS

Patients and sample processing

All research was conducted in accordance with both the Declarations of Helsinki and Istanbul. Patient samples were collected from the National University Hospital (NUH) Singapore, Singapore General Hospital (SGH), and National Cancer Centre Singapore (NCCS), with approval by the NUH and SingHealth Central Institution Review Board (CIRB) (CIRB Ref: 2018/2112 and 2016/2626). Resected tumor and adjacent non-tumor liver tissues were obtained from 37 treatment-naive patients with HCC; each provided written informed consent with the demographic and clinical characteristics described in Supplemental Table S1, http://links.lww.com/HC9/B7. Depending on size, the tumors collected from each patient were dissected into 2-5 sectors, separated by at least 1 cm to account for intratumoral heterogeneity.[10] Adjacent non-tumor liver tissues were at least 2 cm away from the tumor. Each tissue sector was allocated for downstream analysis using cytometry by time-of-flight (CyTOF) and bulk tissue RNA sequencing. Tumorinfiltrating leukocytes were isolated from resected HCC tissue by enzymatic digestion with 500 µg/mL collagenase IV (ThermoFisher, MA) and 50 µg/mL DNase I (Roche, IN) for 30 minutes at 37 °C. The cells were stored in liquid nitrogen with 10% DMSO in fetal bovine serum until further analysis.

Marginal sections (comprising tumor and adjacent normal tissues) from 2 of the 37 patients matched for viral status (HBV-negative), stage (TNM stage III) and grade (Edmonson grade III) were subjected to spatial RNA sequencing. Concurrently, archival formalin-fixed paraffin-embedded (FFPE) tissue microarray (TMA) sections from an independent cohort of 49 treatment-naive patients with resected HCC^[11] were used for multiplexed immunofluorescence (mIF), as described below.

Bulk RNA sequencing of tumor and normal tissues

Total RNA from tumor tissues was isolated using the Picopure RNA-Isolation kit (ThermoFisher, MA), and cDNA was generated using the SMART-Seq v4 Ultra Low Input RNA Kit for Sequencing (Takara Bio, Shiga, Japan). With the Nextera XT DNA Library Prep Kit (Illumina, CA), indexed libraries were created and multiplexed for 2×101 bp-sequencing. Raw reads were aligned to the Human Reference Genome hg19 using STAR. The gene-level expected counts were calculated using RNA-seq by expectation maximization v1.3.0 and filtered for protein-coding genes with > 1 count/million reads in > 5% of the samples. Bulk RNA sequencing (RNA-seq) data from this study were deposited in the European Genomephenome Archive (EGA) under the accession code: EGAS00001003814.

GATA4 gene counts in transcripts per million were obtained for each tissue sample. The fold change (FC) of *GATA4* expression for each tumor sector of each patient was calculated as FC = Tx / N, where Tx refers to the tumor sector (x is the number between 1 and 5), and N refers to the adjacent normal liver tissue of the same patient. Each tumor sector was then classified as GATA4 normal or high (norm/high), $FC \ge 0.5$ or GATA4 low (low), FC < 0.5.

Analyses of differentially expressed genes (DEGs) were performed using the R package, Limma, with the false discovery rate adjusted for multiple testing using the Benjamini-Hochberg method. Functional pathway analyses were performed using the Database for Annotation, Visualization, and Integrated Discovery pathway analysis v.6.8. Significant pathways (Benjamini-Hochberg p-value <0.05) were filtered out, and the top ten functional pathways by fold enrichment were selected for analysis. Known gene markers for tumor progression or immune functions were further identified for visualization.

Cytometry by time-of-flight

Isolated immune cells from tumor and normal adjacent non-tumor liver tissues were stained with 2 CyTOF panels: lymphoid-centric and myeloid-centric (Supplemental Table S2, http://links.lww.com/HC9/B7 and Supplemental Table S3, http://links.lww.com/HC9/B7) to capture the respective subsets. Briefly, immune cells were thawed, stimulated, or unstimulated for 5 hours with phorbol 12-myristate 13-acetate and ionomycin (Sigma Aldrich, MO). Brefeldin A and monensin (eBioscience, CA) were added during the last 3.5 hours of the incubation. The cells were then washed and stained with cisplatin viability stain (DVS Sciences, CA) and anti-human CD45 leukocyte markers conjugated

with lanthanide metal-89, 115, and 172, respectively, a triple-barcode system, as described. [12] The barcoded immune cells were combined and then stained with antibodies targeting surface markers. The cells were fixed with 1.6% paraformaldehyde and permeabilized in 100% methanol to permit intracellular antibody staining. Finally, a DNA intercalator (DVS Sciences, CA) was added for cellular visualization before analysis using a Helios mass cytometer (Fludigm, CA).

Single-cell CyTOF data from each panel were analyzed separately by FlowJo (v.10.8): live single cells (cisplatin-negative and DNA-intercalator-positive) were normalized and de-barcoded to each sample file based on their unique CD45 barcodes as described.[12] The resulting data was down-sampled to 10,000 live immune cells for each group for subsequent dimension reduction and unsupervised clustering using an in-house developed Extended Polydimensional Immunome Characterization analysis pipeline, which contains the browser-based R Shiny app "SciAtlasMiner"[13] for data visualization. Forty-nine clusters were obtained for each panel using a 7×7 FlowSOM clustering algorithm. The clusters were then analyzed for enrichment in either GATA4-Norm/High or -Low for all tumor sectors. Data were further validated by manual gating using FlowJo (v.10.8). Owing to limited availability, a subset of the samples was run on the myeloid-centric panel for CtvTOF.

Spatial transcriptomics

Sample preparation for analysis of mRNA in 2 FFPE sections (GATA4-norm/high vs. GATA4-low) was performed using the Visium spatial pipeline (10X Genomics, CA), according to the manufacturer's instructions. Briefly, 5 μ m FFPE tissue sections were deparaffinized by immersion in xylene, followed by immersion in 100% ethanol, 95% ethanol, 70% ethanol, and Milli-Q water. The slide was then placed in a tissue slide cassette, and de-cross-linking buffer was added to the deparaffinized slide, sealed, and incubated at 95 °C for 1 hour. The sections were then subjected to probe hybridization and ligation. The whole transcriptome probe panel consisted of ~3 pairs of specific probes for each targeted gene, enabling hybridization and ligation of each probe pair.

Tissue slides and Visium CytAssist spatial gene expression slides (10X Genomics, CA) were loaded into the Visium CytAssist instrument (10X Genomics, CA), where they were brought near one another. Visium CytAssist spatial gene expression slides utilize 6.5×6.5 mm capture areas with approximately 5000-oligonucleotide barcoded spots required to capture gene expression probes. Gene expression probes were released from the tissue on CytAssist-enabled RNA digestion and probe release, allowing capture by

spatially barcoded oligonucleotides present on the slide surface. Next, the Visium CytAssist spatial gene expression slide was removed from the Visium CytAssist instrument for downstream library preparation. Gene expression libraries were generated for each tissue section for whole transcriptome sequencing. Spatial barcodes were used to associate the reads back to the tissue section images for the spatial mapping of gene expression. Data available on request from the authors.

Spatial transcriptomics data analysis

The Visium expression matrix for each sample obtained through the Space Ranger 2.0.1 pipeline (10X Genomics, CA), mapped using the GRCh38-2020-A reference transcriptome, was processed using Seurat v4.0.4 (Satija Lab, NY). The Seurat object contains both spot-level expression data and the associated image of the tissue slice. Spots containing more than 3 transcripts (unique molecular identifiers) were defined as valid spots and processed for downstream analysis. Normalization and variable gene detection were performed using the SCTransform function. Spatial gene expression analysis was carried out using the SpatialFeaturePlot function. Clustering and uniform manifold approximation and projection were performed on a Loupe browser (10X Genomics, CA), and clusters were annotated using the Deeply Integrated human Single-Cell Omics scEnrichment tool.[14] Specific features (genes) were analyzed using Seurat 4.0. Normalization was performed using SCTransform.[15] and gene expression was visualized using SpatialFeaturePlot.[16]

Multiplexed immunofluorescence

mIF was performed on FFPE TMA sections of tumor tissues from an independent cohort of 49 patients with HCC. Two samples of tumor were obtained from each patient. FFPE sections were deparaffinized and stained using the OPAL 7-color IHC Kit (Akoya Biosciences, MA). The primary antibodies used for staining were all from Abcam, Cambridge, UK (Supplemental Table S4, http://links.lww.com/HC9/B7): anti-human (EPR6855), anti-human CD11b (EPR1344), anti-human CD33 (SP266), anti-human CCL20 (polyclonal), and anti-human Forkhead box P3 (FoxP3) (236A/E7). The sections were co-stained with DAPI. Images were acquired at room temperature using Vectra 3.0 Pathology Imaging System Microscope (UPlanSAPO 20x/0.75 objective; Olympus, Tokyo, Japan) with the in-built TMA imaging pipeline. Unmixing was performed using InForm v2.1 (Akoya Biosciences, MA), and images were exported through Imaris v9.1.0 (Bitplane, Belfast, UK).

Quantification of CCL20 expression and the densities of CD4 T cells, Tregs, and myeloid-derived suppressor cells (MDSCs) was conducted using ImageJ software. CCL20 expression was quantified as area (mm² per tumor core), whereas the densities of CD4 T cells, Tregs, and MDSCs were quantified as number of cells/mm² using average data from 3 to 5 tumor cores from each patient. Note that 1 mm² was the area of each tumor core.

Data analysis

Data were analyzed using unpaired Student t test (for quantitative reverse transcription polymerase chain reaction), unpaired Mann-Whitney U tests (for CyTOF and mIF data), chi-squared test (for categorical data) and Spearman correlation on GraphPad Prism 9.3.1. Two-tailed p-values were reported. Identification and visualization of the GATA4 binding site on the CCL20 promoter in the HepG2 cell line was performed using Cistrome DB, a chromatin immunoprecipitation sequencing database. [17,18]

Kaplan-Meier analysis of overall survival (OS) of patients with the Cancer Genome Atlas (TCGA) (liver cancer; n=364) was performed using the KMplot. The best-performing threshold was selected as the cutoff [20] based on the tissue expression. The cutoff values for *GATA4* and *CCL20* were 946 (range of expression: 68–6067) and 286 (range of expression: 0–28,000), respectively. Additionally, we classified the TCGA cohort into *GATA4*-low or *GATA4*-high groups based on median *GATA4* expression and investigated the OS of patients with high versus low *CCL20* expression in both groups separately. The cutoff values for *CCL20* were 351 (range of expression: 0–28,000) in the *GATA4*-low tumors and 2066 (range of expression: 0–23,583) in the *GATA4*-high tumors, respectively.

RESULTS

GATA4-low tumors expressed genes related to tumor aggressiveness and immune exhaustion

Resected samples comprising up to 5 tumor sectors and 1 adjacent non-tumor liver tissue sector were collected from 37 patients with treatment-naive HCC (Supplemental Table S1, http://links.lww.com/HC9/B7). Multiple tumor sectors were collected to account for intratumoral heterogeneity as previously reported. [10,21] All tissue sectors were subjected to bulk RNA-seq and *GATA4* gene counts (transcripts per million) were obtained from each tissue sample. The fold change for each tumor sector was calculated by normalizing the *GATA4* expression of the tumor to that of the nontumor-adjacent tissue. Each tumor sector was then individually classified

as GATA4-norm/high (FC \geq 0.5) or GATA4-low (FC < 0.5; Figure 1A). Overall, 31 tumor sectors were classified as GATA4-low, and 102 tumor sectors were classified as GATA4-norm/high. To rule out the possibility of other confounding factors, we showed that the patients were clinically comparable, with no significant difference in any of the clinical parameters, including viral status, stage, or grade, between the GATA4-low and GATA4-norm/high tumors (Supplemental Table S1, http://links.lww.com/HC9/B7).

To assess the role of GATA4 in the TME of each individual tumor sector, we performed DEG analysis on bulk RNA-seg data and compared GATA4-low and GATA4-norm/high tumor sectors. We found that the enriched genes from GATA4-low tumors were associated with poorer prognosis in HCC. Conversely, genes associated with tumor suppression and better prognosis were enriched in GATA4-norm/high tumors. For instance, secreted phosphoprotein 1 (SPP1), mucin 13 (MUC13), heat shock protein family A (Hsp70) member 6 (HSPA6), contactin 1 (CNTN1), cartilage oligomeric matrix protein (COMP), F-box and WD repeat domain containing 10 (FBXW10), matrix metallopeptidase 12 (MMP12), and FXYD domain containing ion transport regulator 3 (FXYD3) have been associated with poorer outcomes or tumor growth in HCC and are expressed in GATA4-low tumors[22-24] (Figure 1B and Supplemental Table S5, http://links.lww.com/HC9/B7). Furthermore, immunosuppressive and exhaustion markers such as Programmed Cell Death 1 (PDCD1) (programmed cell death protein 1 [PD-1]), T-cell immunoreceptor with Iq and ITIM domains (TIGIT), cytotoxic T lymphocyte-associated protein 4 (CTLA4). and hepatitis A virus cellular receptor 2 (HAVCR2) (Tim-3), as well as IL10 were elevated in GATA4-low tumors (Figure 1B and Supplemental Table S5, http://links.lww. com/HC9/B7). In contrast, genes that have been associated with tumor suppression or antitumor activity in HCC, such as crystallin alpha A (CRYAA), t-complex 10 like (TCP10L), betaine-homocysteine S-methyltransferase (BHMT), insulin-like growth factor binding protein acid labile subunit (IGFALS), fibronectin type III domain containing 5 (FNDC5), and hydroxyacid oxidase 2 (HAO2)[25,26] were enriched in GATA4-norm/high HCC tumors (Figure 1B and Supplemental Table S5, http:// links.lww.com/HC9/B7).

Additionally, the DEGs enriched in either group were analyzed for their involvement in various signaling pathways using the Database for Annotation, Visualization, and Integrated Discovery. Significant pathways enriched in *GATA4*-norm/high tumors included processes involved in mitochondrial function and fatty acid beta-oxidation (Figure 1C). Despite the enrichment of a few immune-active pathways, overall the *GATA4*-low tumors were enriched with more immunosuppressive pathways and genes (Supplemental Tables S5, S6, http://links.lww.com/HC9/B7). One such upregulated

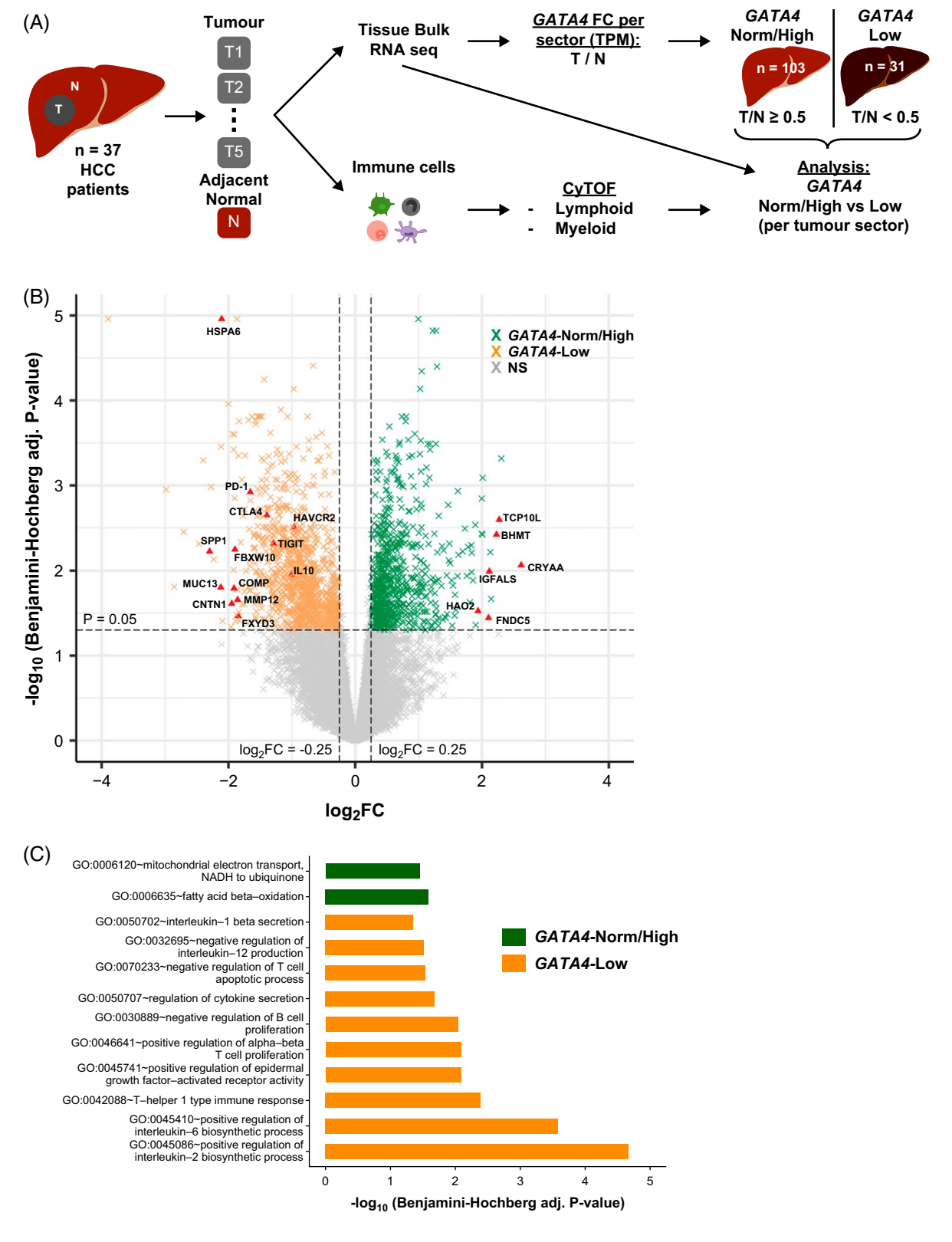


FIGURE 1 Comparison of differentially expressed genes between *GATA4*-norm/high and *GATA4*-low tumors. (A) Two to 5 tumor sectors (T) and 1 adjacent nontumor sector (N) sample were collected from each of the 37 patients with HCC and analyzed by RNA sequencing (seq) and CyTOF for their transcriptomic and immunomic profiles. (B) Volcano plot highlighting the significant genes upregulated in *GATA4*-norm/high and *GATA4*-low from bulk RNA sequencing. (C) Functional pathway analysis of the differentially expressed genes using the Database for Annotation, Visualization, and Integrated Discovery. Abbreviations: BHMT, betaine-homocysteine S-methyltransferase; CNTN1, contactin 1; COMP, cartilage oligomeric matrix protein; CRYAA, crystallin alpha A; CTLA4, cytotoxic T lymphocyte-associated protein 4; CyTOF, cytometry by time-of-flight; FC, fold change; FNDC5, fibronectin type III domain containing 5; FXYD3, FXYD domain-containing ion transport regulator 3; GATA4, GATA binding protein 4; HAO2, hydroxyacid oxidase 2; HAVCR2, hepatitis A virus cellular receptor 2; IGFALS, insulin-like growth factor binding protein acid labile subunit; MUC13, mucin 13; PD-1, programmed cell death protein 1; TCP10L, t-complex 10 like; TIGIT, T cell immunoreceptor with Ig and ITIM domains; TPM, transcripts per million.

pathway in GATA4-low tumors is IL-1b secretion (Figure 1C), which has been reported to be associated with poorer prognosis in various solid tumors such as lung, colon, melanoma, esophageal, and breast cancers.[27,28] Furthermore, the pathway involved in the negative regulation of IL-12 production, a antitumor cytokine, [29] was well-described upregulated GATA4-low tumors (Figure 1C). Similarly, the positive regulation of epidermal growth factor receptor, which is associated with primary resistance to sorafenib, [30] was observed (Figure 1C). Furthermore, previous studies have shown that epidermal growth factor receptor promotes tumor metastasis in vitro and in vivo.[31] Thus, the DEG analysis corroborates the notion that GATA4-low tumors exhibit a tumor subtype with an immunosuppressive microenvironment.

GATA4-low tumors are enriched with immunosuppressive and exhausted lymphoid subsets

To better examine the immune landscapes of the tumors, we next used CyTOF to phenotype lymphoid (lymphoid-centric antibody panel, Supplemental Table S2, http://links.lww.com/HC9/B7) subsets in the TME from GATA4-low and GATA4-norm/high tumors. First, we examined lymphoid immune subsets using the twodimensional t-distributed stochastic neighbor embedding plots generated from the CyTOF data of individual cells clustered based on similarity in their protein markers expression (Supplemental Figure S1A, http:// links.lww.com/HC9/B7). Unpaired Mann-Whitney U test on the proportions of the resulting cell clusters identified 13 lymphocyte clusters that were significantly enriched in either GATA4-norm/high or GATA4low HCC tumors (Figure 2A, B). These clusters were further classified into 4 main immune lineages: CD4 and CD8 T cells, natural killer (NK) cells, and NKT cells (Figure 2A).

Within CD4 T-cell clusters, CTLA4-expressing central memory T cells and regulatory T cells (Tregs) were found to be significantly enriched in GATA4-low tumors (Figure 2C). Furthermore, higher numbers of PD-1+CCR6+ (C-C Motif Chemokine Receptor 6) exhausted CD8 central memory T cells were present in GATA4-low tumors, whereas PD-1- nonexhausted CD8 resident memory T cells were enriched in GATA4norm/high tumors (Figure 2D). Cytotoxic granzyme B (GzmB+) T-box transcription factor TBX21 (Tbet+) NK cells, activated CD69+CD244+ NK, and NKT cells were significantly enriched in GATA4-norm/high tumors (Figure 2E). We further validated the enrichment of each cluster by manual gating using FlowJo (v.10.8.1) (Figure 2C-E and Supplemental Figure S1B, http:// links.lww.com/HC9/B7). These data support the above bulk RNA-seq findings that immunosuppressive or exhausted cells are indeed more prevalent in the *GATA4*-low tumors.

GATA4-low tumors showed enrichment in myeloid-derived suppressor cells and immunosuppressive macrophages

Next, we performed CyTOF analysis specifically on myeloid subsets (myeloid-centric antibody panel; Supplemental Table S3, http://links.lww.com/HC9/B7). CD3+ T cells were excluded before performing unsupervised clustering of myeloid subsets (Supplemental Figure S2A, http://links.lww.com/HC9/B7). We identified 4 clusters of myeloid cells, with further manual gating validation (Supplemental Figure S2B, http://links.lww.com/HC9/B7), that were enriched in GATA4-low tumors (Figure 3A, B). Among them, 3 MDSC subsets, mononuclear MDSCs and polymorphonuclear MDSCs, which are known to be associated with immunosuppression, [32] were found to be significantly enriched in GATA4-low tumors (Figure 3C). V-domain Ig suppressor of T-cell activation (VISTA)+ and tunica intima endothelial kinase 2+ macrophages were also found in higher proportions in GATA4-low tumors (Figure 3C). VISTA has been shown to selectively interact with and suppress T cells in the TME at acidic pH,[33] while TIE2 has been shown to promote tumor vascularization.[34] In contrast, nonclassical monocytes, proinflammatory (CD86+CD11c+) macrophages, and type 2 conventional dendritic cells, which have been associated with a more favorable tumor prognosis and antitumor response, [35-37] were significantly enriched in GATA4-norm/ high tumors (Figure 3D). Therefore, immune profiling revealed that low GATA4 expression in HCC is significantly linked to the enrichment of various myeloid subsets associated with immunosuppression and tumor progression.

GATA4-low tumors express higher levels of immunosuppressive cytokine CCL20

As chemokines are key contributors to an immunosuppressive TME, [38] we next sought to visualize the expression of *GATA4* and its correlation with the chemokine network with spatial transcriptomic analysis. To do this, we performed Visium CytAssist spatial gene expression analysis (10X Genomics) (see Methods section) on 2 representative HCC samples with either *GATA4*-norm/high (HCC1) or *GATA4*-low (HCC2) status. We first performed hematoxylin and eosin staining on FFPE samples to observe tumor morphology and delineate the tumor margins (Figure 4A) before performing spatial transcriptomic analysis on sequential FFPE sections. Average reads of 14,774 and 15,598 per spot were captured for HCC1 and HCC2, respectively. Clustering, annotation,

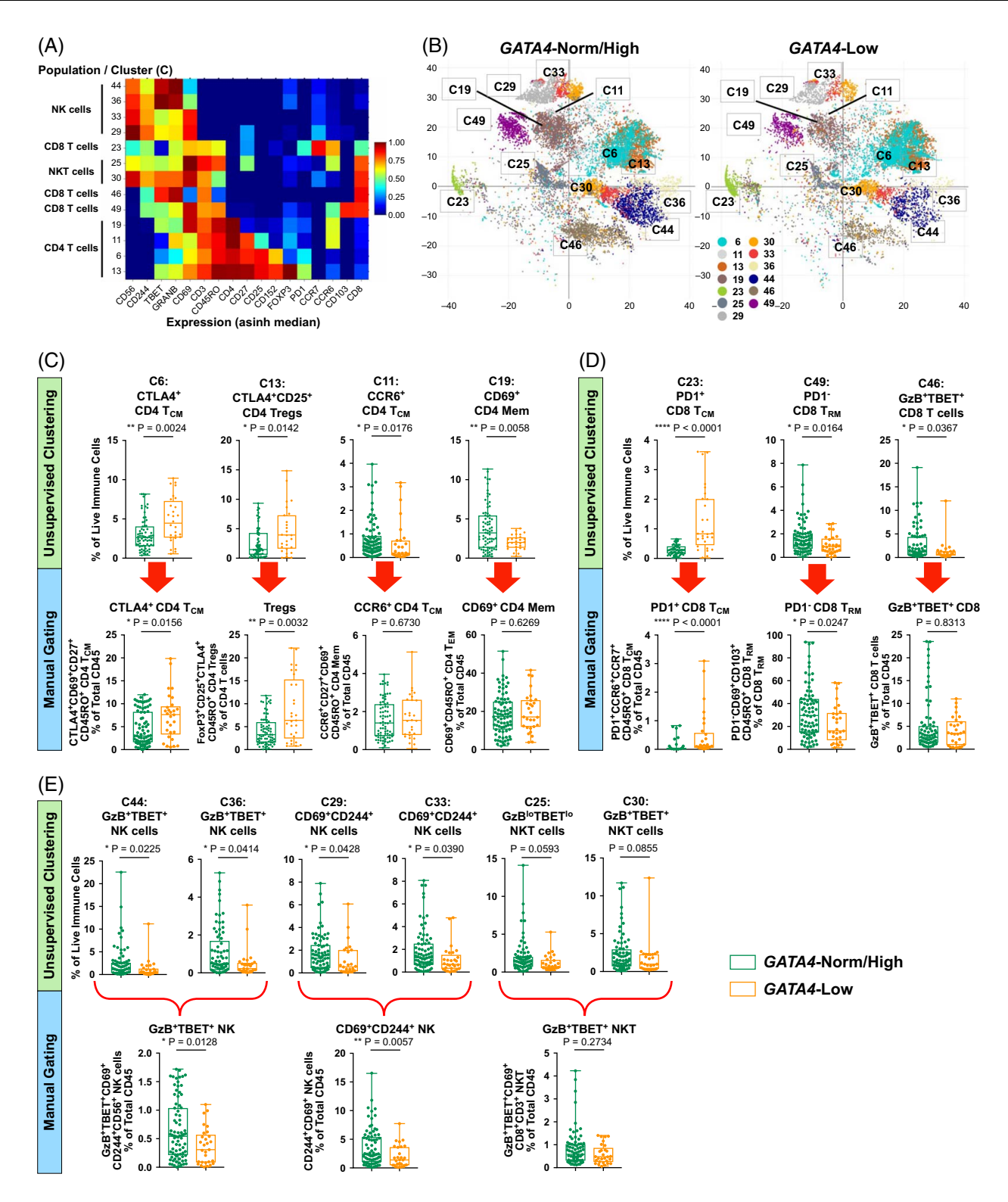


FIGURE 2 Immune profiling of the lymphoid subsets from *GATA4*-norm/high and *GATA4*-low tumors. (A) Median expression of selective immune markers in CD4 T cells, CD8 T cells, NKT cells, and NK cells clusters (C). (B) t-distributed stochastic neighbor embedding plots of the 13 significantly enriched lymphoid clusters (C) in *GATA4*-norm/high or *GATA4*-low tumor sectors. (C–E) Proportions of enriched immune clusters and validation of immune subsets by manual gating using markers as stated on *y*-axis for (C) CD4 T cells, (D) CD8 T cells and (E) NK/NKT cell subsets. Abbreviations: CCR, C-C Motif Chemokine Receptor; FoxP3, Forkhead box P3; GATA4, GATA binding protein 4; NK, natural killer cells; NKT, natural killer T cells; Tbet, T-box transcription factor TBX21; TCM, central memory T cell; Tregs, regulatory T cells; T_{RM}, resident memory T cells.

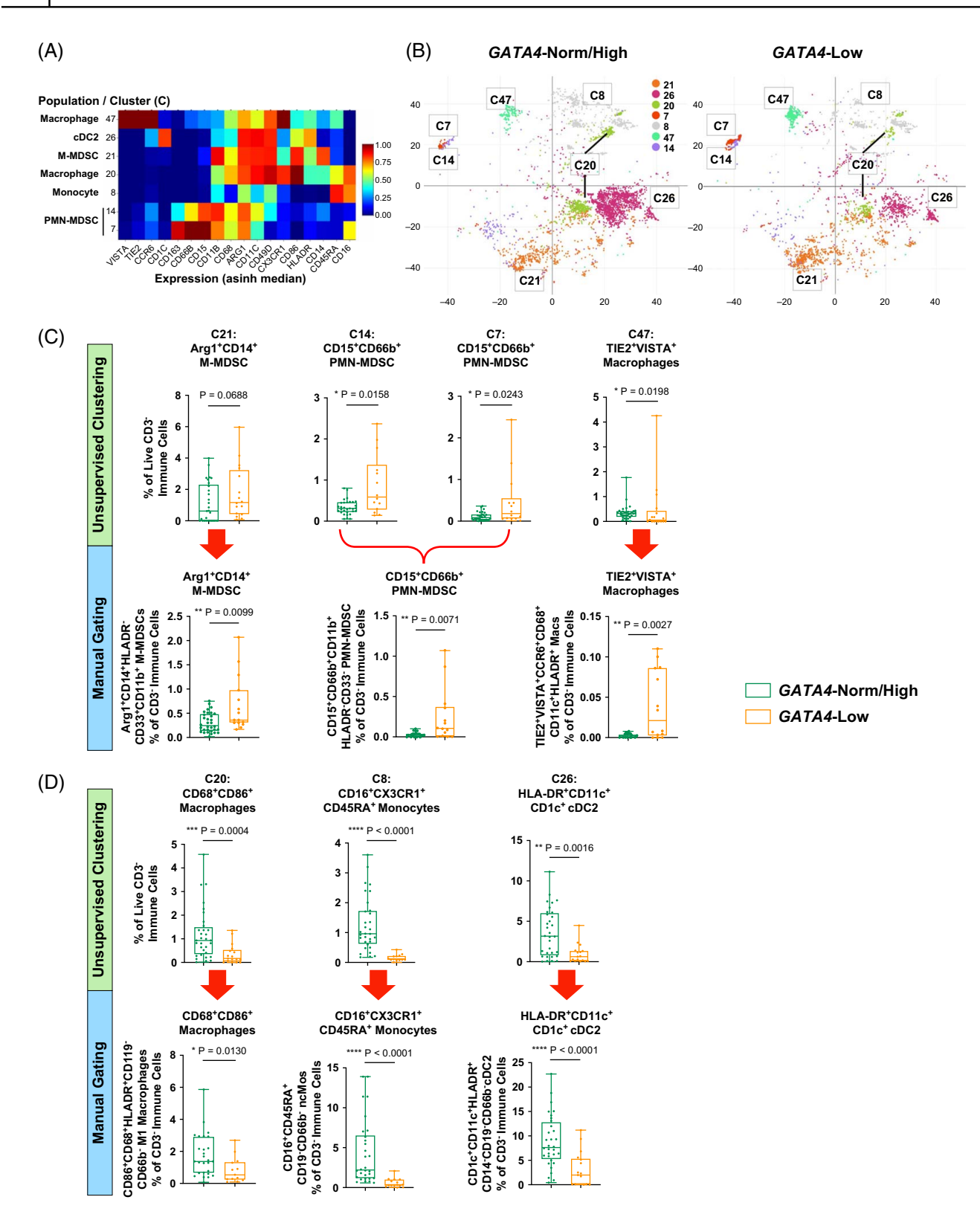


FIGURE 3 Immune profiling of the myeloid subsets from *GATA4*-norm/high and *GATA4*-low tumors. (A) Median expression of immune markers in MDSCs, macrophages, nonclassical monocytes, and cDC2 clusters (C). (B) t-distributed stochastic neighbor embedding plots of the enriched myeloid clusters (C) in *GATA4*-norm/high and *GATA4*-low. (C) Proportions of enriched immune clusters in *GATA4*-low tumors and further validation by manual gating using markers as stated on *y*-axis for MDSCs and immunosuppressive macrophages. (D) Proportions of enriched immune clusters in *GATA4*-norm/high tumors and further validation by manual gating using markers as stated on *y*-axis for ncMos, proinflammatory macrophages, and cDC2. Abbreviations: cDC2, conventional dendritic cells; GATA4, GATA binding protein 4; MDSCs, myeloid-derived suppressor cell; PMN, polymorphonuclear; TIE2, tunica intima endothelial kinase 2; VISTA, V-domain Ig suppressor of T-cell activation.

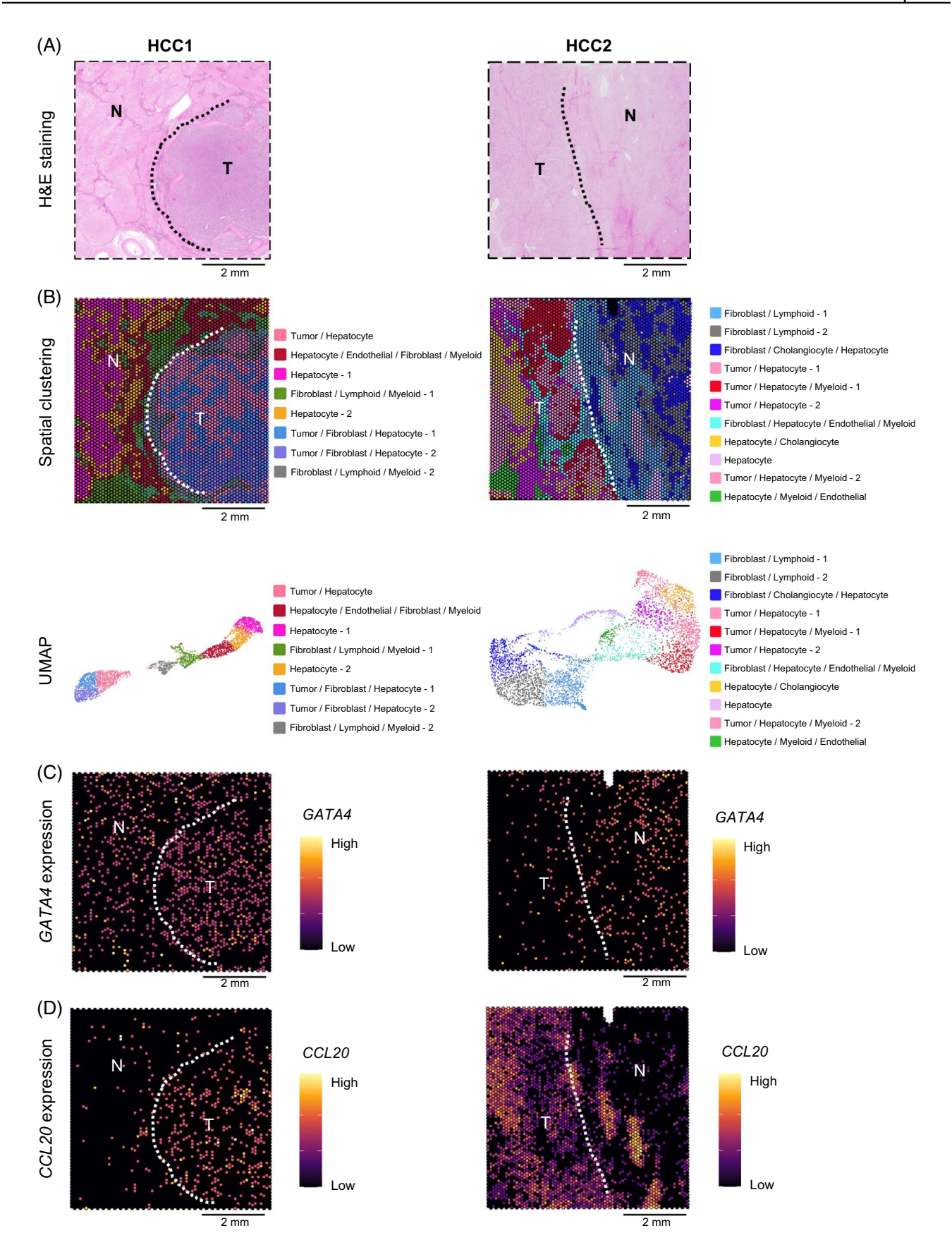


FIGURE 4 Spatial correlation of *GATA4* and *CCL20* in HCC tumors. (A) H&E staining of HCC1 and HCC2 tissues. (B) Clustering and uniform manifold approximation and projections of HCC1 and HCC2 tissues according to spatial RNA expression. (C, D) Images showing the RNA expression of (C) *GATA4* and (D) *CCL20* in the tumor (T) and surrounding non-tumor (NT) tissue (n = 2). Abbreviations: CCL20, C-C Motif Chemokine Ligand 20; GATA4, GATA binding protein 4; H&E, hematoxylin and eosin; N, Non-tumor; T, Tumor.

and uniform manifold approximation and projection were performed based on the spatial RNA expression of the tissues (Figure 4B and Supplemental Table S7, http://links.lww.com/HC9/B7).

We investigated the expression of various cytokines in GATA4-low and GATA4-norm/high samples. Of note, mRNA expression of co-stimulatory cytokines CXCL9, C-X-C Motif Chemokine Ligand 9 (CXCL9) and C-X-C Motif Chemokine Ligand 10 (CXCL10) were higher in HCC1 (GATA4-norm/high) than HCC2 (GATA4-low) (Supplemental Figure S3A, B, http://links.lww.com/ HC9/B7). On the other hand, cytokines associated with tumor progression such as C-C Motif Chemokine Ligand 2 (CCL2)[39] and C-C Motif Chemokine Ligand 21 (CCL21)[40] (Supplemental Figure S3C, D, http:// links.lww.com/HC9/B7) and immunosuppression, C-C Motif Chemokine Ligand 11 (CCL11)[41] (Supplemental Figure http://links.lww.com/HC9/B7) increased at the tumor borders and adjacent "normal" regions of HCC2 (GATA4-low), compared to HCC1 (GATA4-norm/high). Importantly, we observed elevated CCL20 expression in GATA4-low compared to GATA4norm/high particularly in the tumor regions (Figure 4C, D), showing a trend of higher CCL20 expression in regions where GATA4 was lost.

Next, we investigated whether GATA4 downregulation correlated with an increase in CCL20 expression. Indeed, using bulk RNA sequencing, we found that GATA4 RNA expression was inversely correlated with CCL20 RNA expression in the tumors (Figure 5A). To confirm whether CCL20 is indeed a downstream target of GATA4, we utilized a lentiviral system containing the (Dox)-inducible doxycycline GATA4 gene overexpress GATA4 in two HCC cell lines, Huh7 and PLC/PRF/5, both of which express very low baseline levels of GATA4 (Figure 5B and Supplemental Methods, http://links.lww.com/HC9/B7). Using quantitative reverse transcription polymerase chain reaction, we first showed that Dox treatment strongly induced GATA4 overexpression in Huh7 and PLC/PRF/5 cell lines (Figure 5B). We then compared the downregulated genes in GATA4-overexpressed Huh7 and PLC/PRF/5 cells with the upregulated genes in 102 HCC tumors compared to nontumor tissues from our previous HCC cohort study using bulk transcriptomics.[21] We have identified five overlapping genes that were highly expressed in the GATA4-low tumor sectors from our previous HCC cohort data set and downregulated by GATA4 overexpression in the cell lines (Figure 5C), indicating their potential roles in tumor progression.

Using quantitative reverse transcription polymerase chain reaction we validated the reduced *CCL20* expression in Huh7 and PLC/PRF/5 cell lines with concomitant *GATA4* overexpression on Dox treatment (Figure 5D). In addition, publicly accessible chromatin immunoprecipitation sequencing data (from Cistrome Data Browser^[17,18]) has shown that GATA4 binds to the

promoter of *CCL20* in the HepG2 cell line (Supplemental Figure S4, http://links.lww.com/HC9/B7). Combining this with our transcriptomics data above, these indicate that the binding of GATA4 to the *CCL20* promoter site would suppress its transcription and expression. Thus, we show that *CCL20* is a downstream target of GATA4 and a potential chemotactic gene responsible for shaping the immunosuppressive TME mediated by GATA4.

CCL20-high tumors are enriched with Tregs and MDSC subsets

Given the fact that CCL20 contributes to the recruitment and expansion of immunosuppressive cells such as Tregs[8] and MDSCs,[42] and our CyTOF data showed the enrichment of both Tregs and MDSCs in GATA4-low tumors (Figures 2C, 3C), we next examined whether low GATA4 expression could contribute to immunosuppression via mediated Treg and MDSC recruitment to the TME. We gated on Tregs and MDSCs from our CyTOF data (Figures 2C, 3C) and showed that, indeed, their frequencies were positively correlated with the RNA expression of CCL20 in HCC tumors (Figure 6A, B). To further validate this, we performed mIF staining on TMA sections from an independent cohort of 49 patients with HCC with 89 tumor cores (Figure 6C). Tumor cores were separated into CCL20-high or CCL20-low groups based on the median CCL20 protein expression (Figure 6D, G). The numbers of Tregs and MDSCs were quantified and compared between CCL20-high and CCL20-low tumors. We found that, indeed, CCL20-low tumors showed a significant enrichment of Tregs (Figure 6E, H) and MDSCs (Figure 6F, H). CD4+ T cells and the ratio of Tregs to CD4 T cells were also higher in CCL20-high than CCL20-low tumor sections (Supplemental Figure S5A, B, http://links.lww.com/HC9/B7). These results indicate that the recruitment of immunosuppressive cells in the TME observed in GATA4-low tumors is potentially mediated by CCL20.

Patients with *GATA4*-low and *CCL20*-high tumors were associated with poorer OS

As our above data demonstrated that GATA4 reduction is related to tumor aggressiveness and immunosuppression of TME in HCC, we investigated its relevance in the clinical outcomes of patients with HCC. To examine this, we performed Kaplan-Meier survival analysis on the TCGA liver cancer cohort (n = 364) according to their tumor expression of *GATA4* and *CCL20*. Patients with *GATA4*-low tumor expression showed a trend of lower OS than patients with high *GATA4* expression in the tumors (Figure 7A). As GATA4

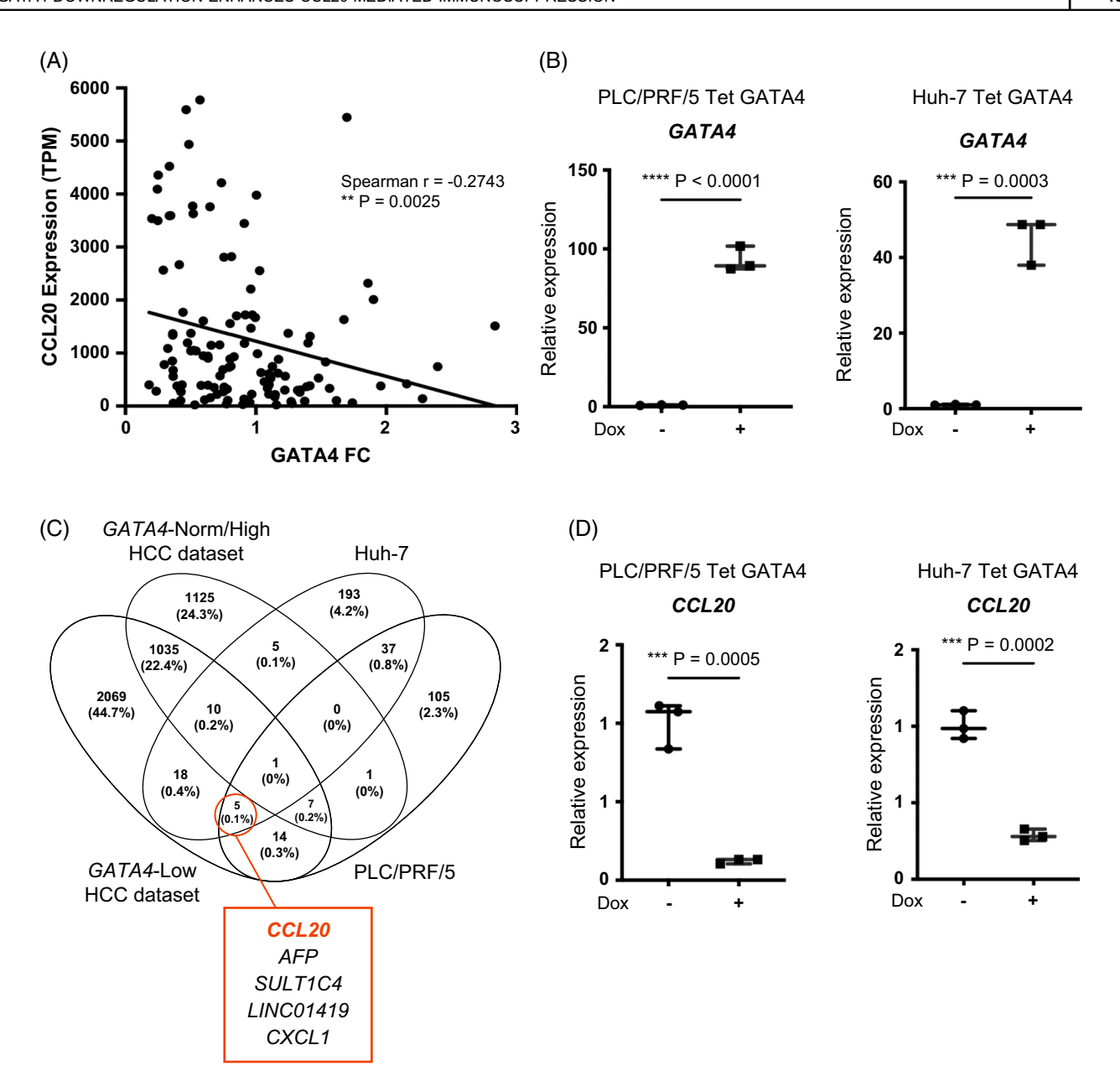


FIGURE 5 Identification of CCL20 as a downstream target of GATA4. (A) Correlation between *GATA4* fold change and *CCL20* expression according to bulk RNA sequencing. (B) Quantitative RT-PCR showing mRNA overexpression of *GATA4* on doxycycline (Dox) treatment in PLC/PRF/5 and Huh-7 cell lines containing lentiviral system with Dox-inducible *GATA4* gene. (C) Venn diagram representing genes downregulated more than 2-fold (adjusted *p*-value < 0.05) in both Dox-treated PLC/PRF/5 and Huh-7 Tet GATA4 cells, overlapped with genes highly expressed in *GATA4*-Low and not *GATA4*-Norm/High tumors from our previous HCC cohort study (PLANet) data set (37). These 5 overlapping genes included *CCL20*. (D) mRNA levels of *CCL20* were reduced on Dox-induced *GATA4* overexpression in PLC/PRF/5 and Huh-7 cell lines, measured by quantitative RT-PCR. Abbreviations: CCL20, C-C Motif Chemokine Ligand 20; CXCL10, C-X-C Motif Chemokine Ligand 10; GATA4, GATA binding protein 4; TPM, transcripts per million.

reduction may exert its immunosuppressive function via corresponding increase in CCL20 as shown by our data above, we also examined the impact of *CCL20* expression on patient survival. Correspondingly, Kaplan-Meier analysis of the TCGA liver cancer cohort showed that patients with *CCL20*-high tumors had lower OS than patients with *CCL20*-low tumors (Figure 7B).

Further survival analyses demonstrated that the survival differences segregated by CCL20 expression

were only significant in patients with *GATA4*-low tumors (Figure 7C) but not in patients with *GATA4*-high tumors (Figure 7D). These findings further emphasize the interaction between GATA4 and CCL20 in HCC progression. In conclusion, our current findings demonstrate the clinical relevance of *GATA4* and *CCL20* in liver cancer prognosis and immunosuppression underscoring their potential importance in future research and therapeutic strategies.

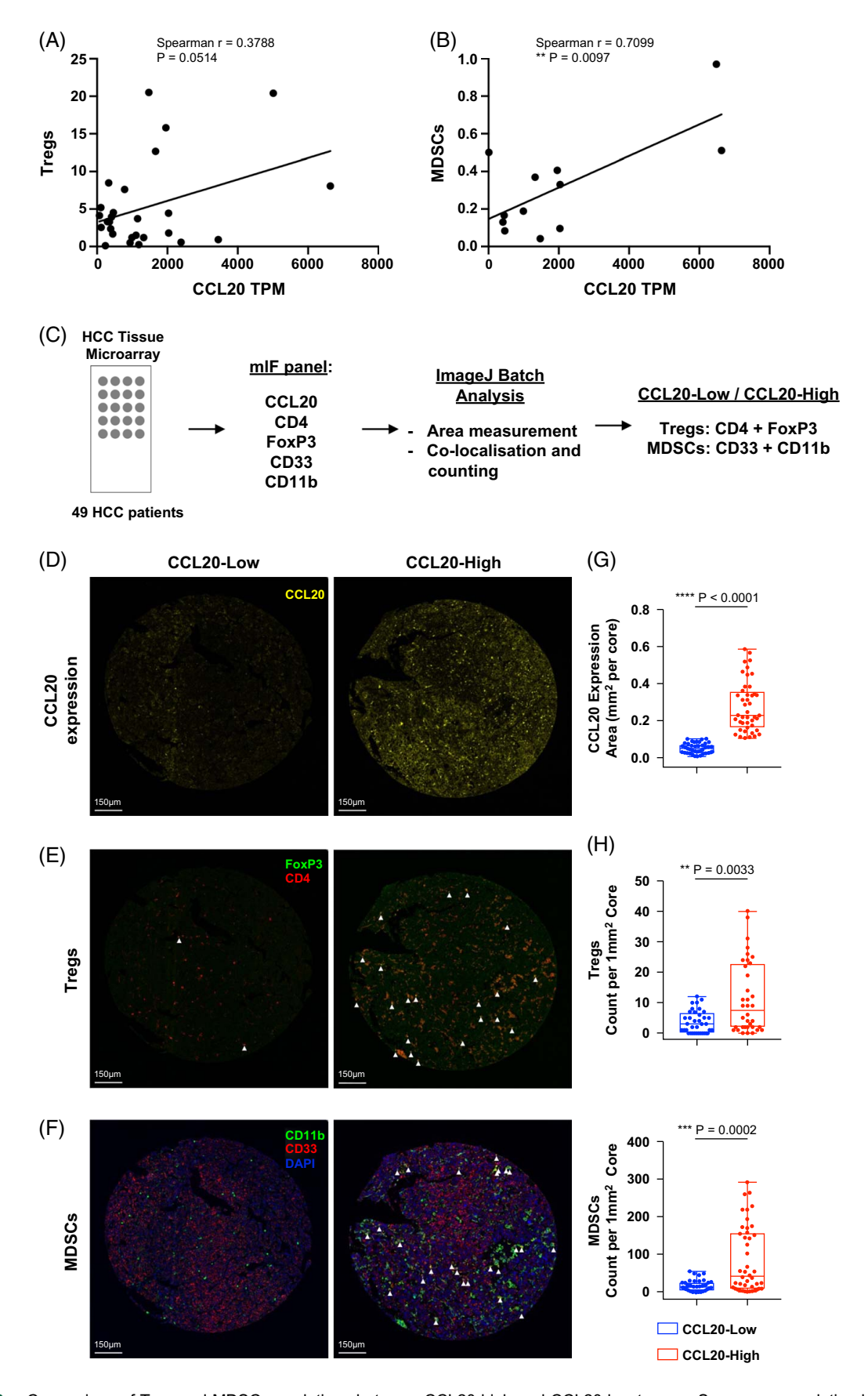


FIGURE 6 Comparison of Treg and MDSC populations between CCL20-high and CCL20-low tumors. Spearman correlation between frequencies of total (A) Treg and (B) MDSC from CyTOF data, with CCL20 gene expression (TPM) from bulk RNA-seq data of matched tumor tissue.

(C) mIF staining was performed on tissue microarray sections from an independent cohort of 49 patients with HCC. (D–F) Representative images showing protein expression of (D) CCL20 (yellow), (E) Tregs (FoxP3=green; CD4=red) as denoted by white arrows and (F) MDSCs (CD11b=green; CD33=red, co-stained with DAPI=blue), all based on their respective median densities. Scale bars: 150 μm. (G) Box plot showing the area of CCL20 expression mm² per core in tumors from CCL20-low and CCL20-high groups. (H) Box plot showing densities of Tregs or MDSCs, quantified as count per 1 mm² core in CCL20-low versus CCL20-high tumors. Abbreviations: CCL20, C-C Motif Chemokine Ligand 20; CyTOF, cytometry by time-of-flight; FoxP3, Forkhead box P3; MDSCs, myeloid-derived suppressor cell; mIF, multiplexed immunofluorescence; TPM, transcripts per million; Tregs, regulatory T cells.

DISCUSSION

GATA4 has been reported to be downregulated in approximately 60% of HCC cases, and studies have shown that the copy number of GATA4 is positively correlated with the number of tumor-infiltrating leukocytes in the tumor. [6,7] In the current study, we found that the TME of GATA4-low HCC tumors exhibited more exhausted immune cells and immunosuppressive cells based on CyTOF analysis. Concurrently, we found that the expression of CCL20 was increased in GATA4-low tumors by correlative analysis and further supported by functional analysis in HCC cell lines. CCL20 is an immunosuppressive chemokine that is highly upregulated in cancers including HCC.[43,44] Our current findings confirm the correlation between high CCL20 expression and accumulation of immunosuppressive subsets, including Tregs and MDSCs, in HCC tumors. To establish a causal relationship between GATA4 and CCL20, we showed that *GATA4* overexpression results in a direct downregulation of CCL20 in vitro, establishing CCL20 as a downstream target of GATA4. Collectively, these results suggest that GATA4 downregulation contributes to an immunosuppressive TME via CCL20.

Our current investigation revealed that the chemokine CCL20, in conjunction with GATA4, contributes to the establishment of an immunosuppressive tumor milieu in HCC. Indeed, CCL20 has been identified in several reports as a potential prognostic marker and therapeutic target for HCC.[44,45] CCL20 can promote cancer progression by inducing tumor cell proliferation and migration via epithelial-mesenchymal transition. [9] Furthermore, tumor-infiltrating CD4⁺ FOXP3⁺ Treg cells could be recruited in a CCL20-CCR6-dependent manner, which was further demonstrated by our findings showing a correlation between CCL20 expression and tumor infiltration of Tregs. Moreover, we found that MDSCs were also enriched in GATA4low CCL20-high tumors. This is consistent with previous studies showing that the CCL20-CCR6 axis mediates the recruitment of multiple immunosuppressive subsets into the TME.[43] Thus, our findings demonstrate the enrichment of immunosuppressive cells via upregulation of the chemokine CCL20, driven by the reduction or loss of GATA4 in HCC tumors.

The current, in-depth exploration of the interplay between GATA4 and immune regulation offers

valuable insights into potential therapeutic strategies for HCC. Harnessing strategies that enhance GATA4 or inhibit CCL20 holds the potential to reverse the observed immunosuppressive mechanisms and enhance the effectiveness of immunotherapy. For instance, *in vivo* studies of cardiotoxicity have shown that treating cardiomyocytes with $\alpha 1$ -adrenergic agonists such as phenylephrine increases GATA4 activity. $^{[46]}$ As such, targeting GATA4 through its activators, such as phenylephrine, or inhibiting CCL20-CCR6 pathways could be considered promising avenues for therapeutic intervention in HCC.

Furthermore, our findings will pave the way for innovative combinatorial therapeutic approaches. Combining anti-CCL20/CCR6 and anti-PD1 treatments could emerge as an appealing immunotherapeutic strategy. By inhibiting the CCL20/CCR6 pathway, we can potentially suppress or even prevent the infiltration of immunosuppressive subsets, thus creating a more favorable TME. Simultaneously, blocking PD-1 can reactivate exhausted CD8⁺ T cells, harnessing their antitumor potential and ultimately contributing to improved clinical outcomes. Indeed, a preclinical study on non-small cell lung carcinoma showed promising outcomes by combining blocking strategies for CCR6 and PD-1 to enhance the therapeutic effect.[47] The enrichment and preferential migration of CCR6+ Tregs to the TME have been previously observed in HCC, contributing to tumor progression.^[8] Additionally, CCR6⁺ B cells have been implicated in HCC progression by promoting angiogenesis.[48] Thus, the potential of anti-CCR6 and anti-PD1 combination therapy as a new immunotherapeutic strategy warrants further exploration in HCC.

In conclusion, our study showed that *GATA4*-low tumors were significantly enriched with immuno-suppressive cells, encompassing both the lymphoid and myeloid subsets. Moreover, our findings revealed a negative correlation between *GATA4* expression and *CCL20*, a chemokine that has previously been linked to immune suppression and unfavorable cancer prognosis. Collectively, these observations underscore the pivotal role of GATA4 loss in facilitating CCL20-mediated immunosuppression. Therefore, we propose GATA4 and CCL20/CCR6 as promising and clinically relevant targets for potential antitumor therapeutic interventions in HCC.

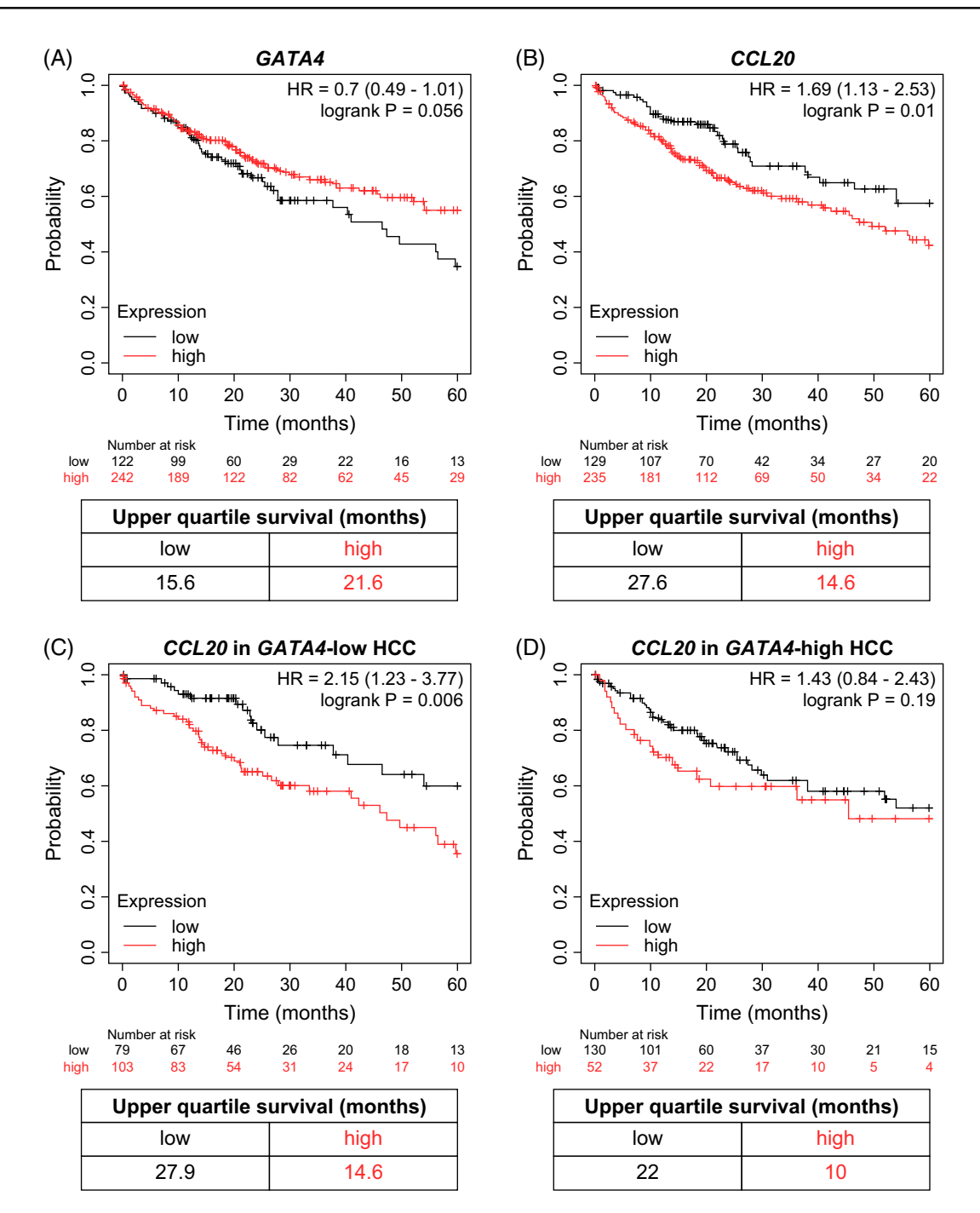


FIGURE 7 Clinical implications of *GATA4* and *CCL20* status in patients with HCC. (A, B) Kaplan-Meier analysis of overall survival profiles of the Cancer Genome Atlas liver cancer cohort (n = 364) segregated by high (red) or low (black) expression of (A) *GATA4* (cutoff value = 946, range of expression: 68–6067) and (B) *CCL20* (cutoff value = 286, range of expression: 0–28000). (C–D) Kaplan-Meier analysis of overall survival profiles of the Cancer Genome Atlas liver cancer cohort segregated by high (red) or low (black) expression of *CCL20* in (C) *GATA4*-low (cutoff value = 351, range of expression: 0–28,000) and (D) *GATA4*-high tumors (cutoff value = 2066, range of expression: 0–23,583). Abbreviations: CCL20, C-C Motif Chemokine Ligand 20; GATA4, GATA binding protein 4.

AUTHOR CONTRIBUTIONS

N. Jannah M. Nasir: investigation, formal analysis, visualization, and writing. Samuel Chuah: investigation and formal analysis. Timothy Shuen: methodology and conceptualization. Rebecca Ba, Aldo Prawira, Mei Chee Lim, and Joelle Chua: investigation and formal analysis. Phuong H. D. Nguyen, Chun J. Lim, Martin

Wasser, and Sharifah N. Hazirah: investigation. Wei Qiang Leow, Tracy Jiezhen Loh, Wei Keat Wan, Yin Huei Pang, Gwyneth Soon, Peng Chung Cheow, Juinn Huar Kam, Shridhar Iyer, Alfred Kow, Yock Young Dan, Glenn K. Bonney: resources. Tony K. H. Lim, Alexander Chung, Brian K. P. Goh, Pierce K. H. Chow, Salvatore Albani, Weiwei Zhai, John F. Ouyang, Han Chong Toh:

resources and supervision. Valerie Chew: conceptualization, funding acquisition, and supervision.

ACKNOWLEDGMENTS

The authors thank all members of TII, all participating patients, and the clinical research coordinators from NCCS, SGH, and NUHS for the contributions to the patient sample collection.

FUNDING INFORMATION

This work was supported by the National Medical Research Council (NMRC), Singapore (reference number: CIRG22jul-0025, NMRC/TCR/015-NCC/2016, NMRC/CSA-SI/0013/2017, NMRC/CSA-SI/0018/2017, NMRC/OFLCG/003/2018), Duke-NUS Khoo Bridge Funding Award (Duke-NUS-KBrFA/2022/0058), International Gilead Sciences Research Scholars Program in Liver Disease—Asia and National Research Foundation, Singapore (ref number: NRF-CRP26-2021-0005). This research was also supported by the Singapore Ministry of Health's National Medical Research Council under its Centre Grant Programme (MOH-000988).

CONFLICTS OF INTEREST

The authors have no conflicts to report.

ORCID

N. Jannah M. Nasir https://orcid.org/0000-0003-3700-9036

Timothy Shuen https://orcid.org/0000-0001-9305-7652

REFERENCES

- Sung H, Ferlay J, Siegel RL, Laversanne M, Soerjomataram I, Jemal A, et al. Global Cancer Statistics 2020: GLOBOCAN estimates of incidence and mortality worldwide for 36 cancers in 185 countries. CA Cancer J Clin. 2021;71:209–49.
- Sangro B, Sarobe P, Hervas-Stubbs S, Melero I. Advances in immunotherapy for hepatocellular carcinoma. Nat Rev Gastroenterol Hepatol. 2021;18:525–43.
- Lu F, Zhou Q, Liu L, Zeng G, Ci W, Liu W, et al. A tumor suppressor enhancing module orchestrated by GATA4 denotes a therapeutic opportunity for GATA4 deficient HCC patients. Theranostics. 2020;10:484–97.
- Kang C, Xu Q, Martin TD, Li MZ, Demaria M, Aron L, et al. The DNA damage response induces inflammation and senescence by inhibiting autophagy of GATA4. Science. 2015;349:aaa5612.
- Xiong H, Hua F, Dong Y, Lin Y, Ying J, Liu J, et al. DNA damage response and GATA4 signaling in cellular senescence and aging-related pathology. Front Aging Neurosci. 2022;14:933015.
- Enane FO, Shuen WH, Gu X, Quteba E, Przychodzen B, Makishima H, et al. GATA4 loss of function in liver cancer impedes precursor to hepatocyte transition. J Clin Invest. 2017; 127:3527–42.
- Patel RS, Romero R, Watson EV, Liang AC, Burger M, Westcott PMK, et al. A GATA4-regulated secretory program suppresses

- tumors through recruitment of cytotoxic CD8 T cells. Nat Commun. 2022;13:256.
- Chen KJ, Lin SZ, Zhou L, Xie HY, Zhou WH, Taki-Eldin A, et al. Selective recruitment of regulatory T cell through CCR6-CCL20 in hepatocellular carcinoma fosters tumor progression and predicts poor prognosis. PLoS One. 2011;6:e24671.
- Ye LY, Chen W, Bai XL, Xu XY, Zhang Q, Xia XF, et al. Hypoxiainduced epithelial-to-mesenchymal transition in hepatocellular carcinoma induces an immunosuppressive tumor microenvironment to promote metastasis. Cancer Res. 2016;76: 818–30.
- Nguyen PHD, Ma S, Phua CZJ, Kaya NA, Lai HLH, Lim CJ, et al. Intratumoural immune heterogeneity as a hallmark of tumour evolution and progression in hepatocellular carcinoma. Nat Commun. 2021;12:227.
- Lee YH, Chuah S, Nguyen PHD, Lim CJ, Lai HLH, Wasser M, et al. IFNgamma(-)IL-17(+) CD8 T cells contribute to immunosuppression and tumor progression in human hepatocellular carcinoma. Cancer Lett. 2023;552:215977.
- Lai L, Ong R, Li J, Albani S. A CD45-based barcoding approach to multiplex mass-cytometry (CyTOF). Cytometry A. 2015;87: 369–74.
- Caicedo HH, Hashimoto DA, Caicedo JC, Pentland A, Pisano GP. Overcoming barriers to early disease intervention. Nat Biotechnol. 2020;38:669–73.
- Li M, Zhang X, Ang KS, Ling J, Sethi R, Lee NYS, et al. DISCO: A database of Deeply Integrated Human Single-Cell Omics data. Nucleic Acids Res. 2022;50(D1):D596–602.
- Hafemeister C, Satija R. Normalization and variance stabilization of single-cell RNA-seq data using regularized negative binomial regression. Genome Biol. 2019;20:296.
- Hao Y, Hao S, Andersen-Nissen E, Mauck WM, Zheng S, Butler A, et al. Integrated analysis of multimodal single-cell data. Cell. 2021;184:3573–87 e3529.
- Zheng R, Wan C, Mei S, Qin Q, Wu Q, Sun H, et al. Cistrome Data Browser: Expanded datasets and new tools for gene regulatory analysis. Nucleic Acids Res. 2019;47(D1):D729–35.
- Davis CA, Hitz BC, Sloan CA, Chan ET, Davidson JM, Gabdank I, et al. The Encyclopedia of DNA elements (ENCODE): Data portal update. Nucleic Acids Res. 2018;46(D1):D794

 –801.
- Menyhart O, Nagy A, Gyorffy B. Determining consistent prognostic biomarkers of overall survival and vascular invasion in hepatocellular carcinoma. R Soc Open Sci. 2018;5:181006.
- Lanczky A, Gyorffy B. Web-Based Survival Analysis Tool Tailored for Medical Research (KMplot): Development and Implementation. J Med Internet Res. 2021;23:e27633.
- Zhai W, Lai H, Kaya NA, Chen J, Yang H, Lu B, et al. Dynamic phenotypic heterogeneity and the evolution of multiple RNA subtypes in hepatocellular carcinoma: the PLANET study. Natl Sci Rev. 2022;9:nwab192.
- Dai Y, Liu L, Zeng T, Liang JZ, Song Y, Chen K, et al. Overexpression of MUC13, a poor prognostic predictor, promotes cell growth by activating Wnt signaling in hepatocellular carcinoma. Am J Pathol. 2018;188:378–91.
- Ng KTP, Qi X, Kong KL, Cheung BYY, Lo CM, Poon RTP, et al. Overexpression of matrix metalloproteinase-12 (MMP-12) correlates with poor prognosis of hepatocellular carcinoma. Eur J Cancer. 2011;47:2299–305.
- Li GY, Huang M, Pan TT, Jia WD. Expression and prognostic significance of contactin 1 in human hepatocellular carcinoma. Onco Targets Ther. 2016;9:387–94.
- Mattu S, Fornari F, Quagliata L, Perra A, Angioni MM, Petrelli A, et al. The metabolic gene HAO2 is downregulated in hepatocellular carcinoma and predicts metastasis and poor survival. J Hepatol. 2016;64:891–.
- 26. Jin B, Gong Z, Yang N, Huang Z, Zeng S, Chen H, et al. Downregulation of betaine homocysteine methyltransferase

(BHMT) in hepatocellular carcinoma associates with poor prognosis. Tumour Biol. 2016;37:5911–7.

- Chen MF, Lu MS, Chen PT, Chen WC, Lin PY, Lee KD. Role of interleukin 1 beta in esophageal squamous cell carcinoma. J Mol Med (Berl). 2012;90:89–100.
- Ding X, Zhang J, Shi M, Liu D, Zhang L, Zhang R, et al. High expression level of interleukin-1beta is correlated with poor prognosis and PD-1 expression in patients with lung adenocarcinoma. Clin Transl Oncol. 2021;23:35–42.
- Colombo MP, Trinchieri G. Interleukin-12 in anti-tumor immunity and immunotherapy. Cytokine Growth Factor Rev. 2002;13: 155–68.
- Ezzoukhry Z, Louandre C, Trécherel E, Godin C, Chauffert B, Dupont S, et al. EGFR activation is a potential determinant of primary resistance of hepatocellular carcinoma cells to sorafenib. Int J Cancer. 2012;131:2961–9.
- Song S, Yu Z, You Y, Liu C, Xie X, Lv H, et al. EGFR/MET promotes hepatocellular carcinoma metastasis by stabilizing tumor cells and resisting to RTKs inhibitors in circulating tumor microemboli. Cell Death Dis. 2022;13:351.
- Li K, Shi H, Zhang B, Ou X, Ma Q, Chen Y, et al. Myeloid-derived suppressor cells as immunosuppressive regulators and therapeutic targets in cancer. Signal Transduct Target Ther. 2021;6: 362.
- Johnston RJ, Su LJ, Pinckney J, Critton D, Boyer E, Krishnakumar A, et al. VISTA is an acidic pH-selective ligand for PSGL-1. Nature. 2019;574:565–70.
- 34. Poh AR, Ernst M. Targeting acrophages in cancer: From bench to bedside. Front Oncol. 2018;8:49.
- Padgett LE, Marcovecchio PM, Olingy CE, Araujo DJ, Steel K, Dinh HQ, et al. Nonclassical monocytes potentiate anti-tumoral CD8(+) T cell responses in the lungs. Front Immunol. 2023;14:1101497.
- Murphy TL, Murphy KM. Dendritic cells in cancer immunology. Cell Mol Immunol. 2022;19:3–13.
- Cendrowicz E, Sas Z, Bremer E, Rygiel TP. The role of macrophages in cancer development and therapy. Cancers (Basel). 2021;13:1946.
- Nagarsheth N, Wicha MS, Zou W. Chemokines in the cancer microenvironment and their relevance in cancer immunotherapy. Nat Rev Immunol. 2017;17:559–72.
- Xu M, Wang Y, Xia R, Wei Y, Wei X. Role of the CCL2-CCR2 signalling axis in cancer: Mechanisms and therapeutic targeting. Cell Prolif. 2021;54:e13115.

- Tutunea-Fatan E, Majumder M, Xin X, Lala PK. The role of CCL21/CCR7 chemokine axis in breast cancer-induced lymphangiogenesis. Mol Cancer. 2015;14:35.
- 41. Wang R, Huang K. CCL11 increases the proportion of CD4 +CD25+Foxp3+ Treg cells and the production of IL-2 and TGF-beta by CD4+ T cells via the STAT5 signaling pathway. Mol Med Rep. 2020;21:2522–32.
- Zhang R, Dong M, Tu J, Li F, Deng Q, Xu J, et al. PMN-MDSCs modulated by CCL20 from cancer cells promoted breast cancer cell stemness through CXCL2-CXCR2 pathway. Signal Transduct Target Ther. 2023;8:97.
- 43. Kadomoto S, Izumi K, Mizokami A. The CCL20-CCR6 axis in cancer progression. Int J Mol Sci. 2020;21:5186.
- Yang X, Ran R, Du J, Qiu Z, Cui L, Jiang X, et al. CCL20 is overexpressed in hepatocellular carcinoma with bile duct tumor thrombus and correlates negatively with surgical outcome. Int J Clin Exp Pathol. 2018;11:3977–83.
- Chew V, Lai L, Pan L, Lim CJ, Li J, Ong R, et al. Delineation of an immunosuppressive gradient in hepatocellular carcinoma using high-dimensional proteomic and transcriptomic analyses. Proc Natl Acad Sci U S A. 2017;114:E5900–9.
- Aries A, Paradis P, Lefebvre C, Schwartz RJ, Nemer M. Essential role of GATA-4 in cell survival and drug-induced cardiotoxicity. Proc Natl Acad Sci U S A. 2004;101:6975–80.
- 47. Wang J, Wang Y, Pan H, Zhao L, Yang X, Liang Z, et al. Chemokine receptors CCR6 and PD1 blocking scFv E27 enhances anti-EGFR CAR-T therapeutic efficacy in a preclinical model of human non-small cell lung carcinoma. Int J Mol Sci. 2023;24:5424.
- He HWJ, Zang M, Wang W, Chang X, Chen X, Wang R, et al. CCR6+ B lymphocytes responding to tumor cell-derived CCL20 support hepatocellular carcinoma progression via enhancing angiogenesis. Am J Cancer Res. 2017;7:1151–63.

How to cite this article: Nasir NJM, Chuah S, Shuen T, Prawira A, Ba R, Lim MC, et al. GATA4 downregulation enhances CCL20-mediated immunosuppression in hepatocellular carcinoma. Hepatol Commun. 2024;8:e0508. https://doi.org/10.1097/HC9.000000000000000000